Comparison of nonlinear 1½-layer and 2½-layer numerical models with strong offshore winds and the Tsushima Current in the East Sea

Soon Young Kim[1], Hyong Sun Lee[2], Dughong Min[3], and Hong-Joo Yoon[4]

[1]Korea Inter-Univ. Institute of Ocean Science, Pukyong National University,
Pusan 608-737, Korea
[2]Dept. Oceanography, Korea Naval Academy, Chinhae 645-797, Korea
[3]Dept. Oceanography, Texas A&M University, College Station TX 77843, USA
[4]Dept. Ocean Engineering, Division of Ocean Systems, Yosu National University,
Yosu 550-749, Korea

According to numerical experiments, the Sokcho Eddy is produced at 37.5~39.0°N by strong offshore winds, whereas the Ulleung Eddy is produced at 35.0~37.0°N by an inflow variation of the Tsushima Current. These locations compare well with visual observations. The nonlinear 1½-layer model showed that most of the East Korea Warm Current (EKWC) driven by the Tsushima Current form the Ulleung Eddy that is larger and stronger than the Sokcho Eddy. In contrast, the nonlinear 2½-layer model showed that most of the EKWC travels further northward due to a strong subsurface current, thereby enhancing the Sokcho Eddy making it larger and stronger than the Ulleung Eddy. The Sokcho Eddy is also produced relatively offshore due to an eastward subsurface current in the frontal region. Using the 1½-layer model, when the mass of the Tsushima Current decreases, the two eddies are weakened and produce a circular shape. In the 2½-layer model the EKWC pushes the Ulleung Eddy northward after 330 days, next the Sokcho and Ulleung eddies begin to interact with each other, and then after 360 days the Ulleung Eddy finally disappears absorbed by the relatively stronger Sokcho Eddy. This behavior compares favorably with other visual observations.

Key words : Sokcho Eddy, Ulleung Eddy, 1½-layer and 2½-layer numerical models, offshore winds, Tsushima Current, East Korean Warm Current

1. Introduction

In general, the upper layer of the East Sea is divided into a warm water region in the southern part and a cold water region in the northern part. A polar front is formed between these water masses at a latitude of approximately 38~40°N. Many small-scale eddies, less than 100 km in diameter, form along this polar front. A strong mesoscale variability also appears in the upper layer of the East Sea. From satellite AVHRR images and velocity distributions, two anticyclonic eddies of about 150~200 km in diameter, called the Sokcho Eddy and Ulleung Eddy, can be observed off the East Coast of Korea (Kim, 1993; Kim, 1995; Shin et al., 1995; Lee et al., 1995; Min et al., 1995).

Recently, there have been several studies of the mechanisms affecting the formation of these eddies (Lie et al., 1995; Lim and Kim, 1995; Kim et al., 1997a and b; 1998). According to Lie et al. (1995), the Ulleung Eddy may be formed by the meandering EKWC, which tends to flow along the isobaths to conserve its potential vorticity. This phenomenon would then seem to cause an omega-shaped me-

ander that eventually forms a warm eddy. The eddy in the Ulleung Basin also seems to weaken and disappear when the inflow of the EKWC decreases. In contrast, Wang(1987) showed that the strait surface outflow generates an anticyclonic eddy after passing through the strait due to nonlinear self-advection. Accordingly, the Ulleung Eddy could be generated by the seasonal change of the Tsushima Current or its nonlinear self-advection. On the other hand, Lim and Kim(1995) studied the inter-action of the Ulleung Warm Eddy using a nonlinear quasi-geostrophic model. The demonstrated the crucial role of topographic effects in the eddy mo-tion process. They showed that the eddy is devel-oped by a nonlinear advection term and dispersion mechanism. However, this study only focuses on the Ulleung Eddy, the Sokcho Eddy and its relation to the Ulleung Eddy was not considered. Kim *et al.* (1997a and b; 1998) analyzed the generating mechanisms of both eddies and highlighted the importance of offshore winds and variations in the Tsushima Current for the Sokcho and Ulleung Eddies, respectively. In their study they used a 1½-layer model, allowing for one active layer above the infinitely deep motionless layer, and carried out three different schemed numerical experiments on the two eddies including an offshore wind study, polar front study, and Tsushima Current study. As a result, the Sokcho Eddy was generated to be mainly due to strong offshore winds and the Ulleung Eddy mainly due to the inflow of the Tsushima Current. However, the interaction bet-ween the upper and lower layers and role of the subsurface current were not examined by the nonlinear 1½-layer model. Furthermore, although the real observation of thes phenomena is unclear, it is necessary to investigate the interaction between the Sokcho and Ulleung Eddies because the warm water of the East Sea is supplied by the Tsushima Current through the Korea Strait, and both Sokcho and Ulleung eddies seem to be strengthened by the warm streamer of the EKWC after formation. Accordingly, the objective of this research is to study the relationship between the Sokcho and Ulleung Eddies and the Tsushima Current, the actual interaction between the two eddies, and finally the combined effect of the Tsushima Current and offshore winds on the two eddies. Nonlinear 1½-layer and 2½-ayer numerical l models were used for the study, and the results compared.

2. Model Ocean

2.1. Equations of motion

2.1.1. Nonlinear 1½-layer model

The nonlinear 1½-layer model has a single, active layer of density ρ_1 overlying a deep, inert layer of density ρ_2 where the pressure gradient is set to zero. This model is very similar to the nonlinear 2½-layer model described by McCreary and Kundu(1988), except that it involves only one active layer.

The equations of motion are as follows:

$$(hu)_t + (uhu)_x + (vhu)_y - fhv + hp_x = \tau^x + \nu_h \nabla^2(hu),$$

$$(hv)_t + (uhv)_x + (vhv)_y + fhu + hp_y = \tau^y + \nu_h \nabla^2(hv),$$

(1a)

$$h_t + (hu)_x + (hv)_y = w_e,$$

$$T_t + uT_x + vT_y = Q/h - w_e(T - T_d)/h + k_h \nabla^2 T,$$

and the pressure gradient is

$$\nabla p = \varepsilon g \nabla [h(T - T_d)] - \frac{1}{2} \varepsilon g h \nabla T. \quad (1b)$$

In these equations, u and v are the zonal and meridional components of the current velocity, re-spectively, the instantaneous thickness of the surface layer is h, its initial value is h, p is the pressure in the layer, f is the coriolis parameter, ν_h is the coefficient of the horizontal eddy viscosity, and g is the acceleration of gravity. The ocean can be forced by either a meridional wind field τ^y or a zonal wind field τ^x. The quantities T and T_d are the temperatures in the surface layer and deep ocean, respectively, and T_d remains constant. ε is the coefficient of thermal expansion. Q, k_h, and w_e are the heat flux through the ocean surface, the horizontal diffusion of heat, and the velocity of entrainment, respectively, and these thre ther-modynamic processes affect T.

The surface heat flux is given by

$$Q = \frac{H}{t_h}(T_0 - T) \qquad (1c)$$

where T_0 is the initial value of T and t_h is a measure of the e-folding time for the upper-layer temperature to relax back to T_0.

Entrainment is a crucial process in this model. It acts to cool the upper layer, provide stress at its bottom, and prevent the interface between the two layers from surfacing. Entrainment is defined by the choice of the entrainment velocity w_e, and, following McCreary and Kundu(1988), a smooth function was adopted:

$$w_e = \begin{cases} (H_e - h)^2/(t_e H_e), & h < H_e, \\ 0 & , \text{ otherwise.} \end{cases} \qquad (1d)$$

According to (1d), entrainment occurs only when h is less than a specified value H_e, and w_e increases parabolically toward the maximum value of H_e/t_e as h goes to zero, where H_e is the starting depth of entrainment and t_e is the thermodynamic time constant. The selected entrainment time scale t_e must be small enough to ensure that the interface does not surface in regions of intense upwelling.

2.1.2. The nonlinear 2½-layer model

This model is a generalization of the preceding 1½-layer model that has two active layers, and is essentially the same model as the one used by McCreary and Kundu(1988). The equations of motion in the upper-layer, denoted by 1, are as follows:

$$(h_1 u_1)_t + (u_1 h_1 u_1)_x + (v_1 h_1 u_1)_y - f h_1 v_1 +$$
$$h_1 p_{1x} = \tau^x + w_e u_2 + \nu_h \nabla^2(h_1 u_1),$$

$$(h_1 v_1)_t + (u_1 h_1 v_1)_x + (v_1 h_1 v_1)_y + f h_1 u_1 +$$
$$h_1 p_{1y} = \tau^y + w_e v_2 + \nu_h \nabla^2(h_1 v_1),$$

$$h_{1t} + (h_1 u_1)_x + (h_1 v_1)_y = w_e. \qquad (2a)$$

$$T_{1t} + u_1 T_{1x} + v_1 T_{1y} =$$
$$Q/h_1 - w_e(T_1 - T_e)/h_1 + k_h \nabla^2 T_1.$$

and the lower layer equations, denoted by 2, are

$$(h_2 u_2)_t + (u_2 h_2 u_2)_x + (v_2 h_2 u_2)_y - f h_2 v_2 +$$
$$h_2 p_{2x} = - w_e u_2 + \nu_h \nabla^2(h_2 u_2),$$

$$(h_2 v_2)_t + (u_2 h_2 v_2)_x + (v_2 h_2 v_2)_y + f h_2 u_2 +$$
$$h_2 p_{2y} = - w_e v_2 + \nu_h \nabla^2(h_2 v_2),$$

$$h_{2t} + (h_2 u_2)_x + (h_2 v_2)_y = - w_e. \qquad (2b)$$

$$T_{2t} = 0.$$

The pressure gradient in the two layers is given by

$$\nabla p_1 = \varepsilon g \nabla[h_1(T_1 - T_3) + h_2(T_2 - T_3)]$$
$$- \frac{1}{2} \varepsilon g h_1 \nabla T_1,$$

$$\nabla p_2 = \varepsilon g(T_2 - T_3)\nabla(h_1 + h_2), \qquad (2c)$$

where T_3 is the temperature of the deep ocean. The surface heat flux Q and entrainment velocity w_e are the same as those in (1c) and (1d), yet with the addition of subscript 1 to H, h, and T.

2.2. Basins and boundary conditions

The model ocean selected was as similar to the East Sea as possible, accordingly, the ocean basin for the numerical solutions was 1200 km zonally and 770 km (about 7^0) meridionally, as shown in Fig. 1. The numerical solutions assumed a rectangular basin, with the western and northern boundaries representing the east coasts of Korea and Russia, respectively, and the southern and eastern boundaries corresponding to the coast of Japan.
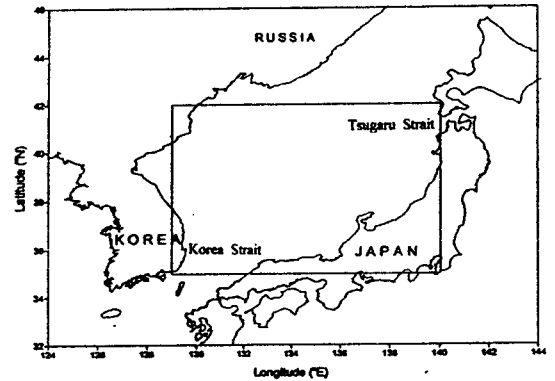

Fig. 1. Idealization of domain of numerical model ocean with the rectangular.

In this numerical study, the inflow of the Tsushima Current with seasonal variations was allowed for, as in Kim et al. (1997a). The Tsushima Current entered the model ocean through a 120 km entry width located at the western corner of the southern boundary and it flowed out through an exit of the same width at the eastern boundary. In the 2½-layer model, an inflow and outflow conditions were imposed on open boundaries in the upper and lower

layers. Fig. 2 illustrates the spatial and temporal structures of the inflow through the entrance of the model ocean. The temporal structure consisted of a larger inflow in the upper layer (V_u) and a smaller one in the lower layer (V_i) with $t=0$ corresponding to December 1. V_u was constant with 20 cms^{-1} for the first 90 days, thereafter, it increased linearly from 20 cms^{-1} to 35 cms^{-1} for 2 months until day 150, at this point it remained steady with a constant speed of 35 cms^{-1} for 4 months until day 270, and finally it decreased from 35 cms^{-1} to 20 cms^{-1} over 3 months until day 360. The temporal variation of V_i was also the same as that of V_u except that its maximum and minimum speeds were 18 cms^{-1} and 3 cms^{-1}, respectively. In the 1½-layer model, the temporal and spatial structures were the same as those in the 2½-layer model except that the maximum speed of its upper layer was 50 cms^{-1}. The actual velocity value to be imposed on the southern open boundary was the velocity scale in Fig. 2(a) times the current velocity V_u or V_i in Fig. 2(b).

Open boundary conditions, as defined by equation(3a), were applied at the southern entrance and eastern exit, whereas, close boundary conditions(3b) were applied elsewhere.

$$u_n = v_n = 0, \quad T_n = 0, \quad h_n = 0 \qquad (3a)$$

$$u = v = 0, \quad T_n = 0, \quad h_n = 0 \qquad (3b)$$

where the subscript n indicates a partial derivative in the normal direction to the boundary, and the conditions of T and h in the equations (3) are based on heat flux and mass conservation.

2.3. Numerical scheme and choice of parameters

The numerical solutions were evaluated on a staggered grid with a rectangular grid box of $\triangle x$ by $\triangle y$. The points for the h and T values were located in the middle of the grid box, and the points for u and v were centered on their meridional and zonal edges, respectively. The equations of motion were forward differenced in time using the leap-frog scheme, and all fields were averaged between two time levels every 40 time steps in order to control any time-splitting instability. The
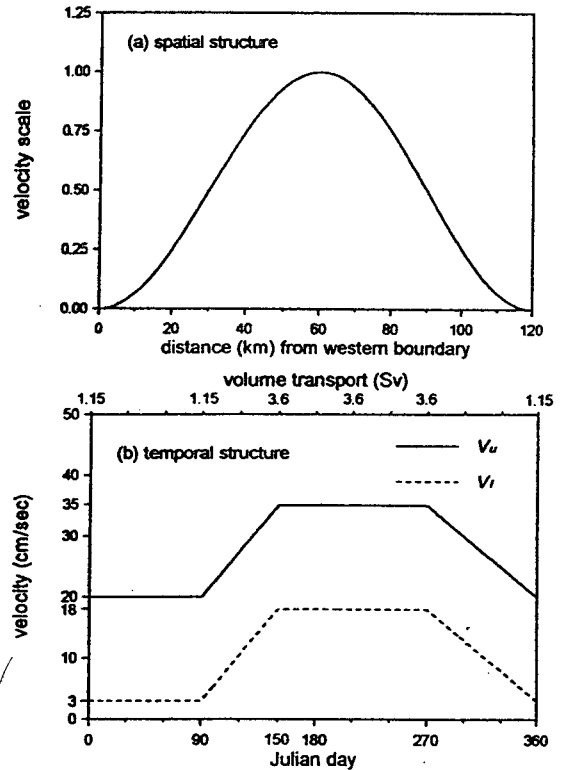

Fig. 2. A schematic diagram illustrating the spatial (a) and temporal (b) structure of the inflow of the Tsushima Current.

diffusive terms were evaluated at the backward time level and all other terms at the central time level, as with McCreary *et al.* (1989).

For all the solutions shown in the figures, the grid dimensions were $\triangle x = \triangle y = 10$ km and the time step $\triangle t = 20$ min. The selected time step was small enough to satisfy the CFL conditions $\triangle t \leq \triangle x/2 \sqrt{2c}$, where c is the free wave speed.

The parameters for the present numerical study are listed in Table 1. Their values were chosen as realistic reflections of the observational data for 1992 (Lee *et al.* 1995) and the mean oceanographic charts of the adjacent seas of Korea published by the National Fisheries Research and Development Agency of Korea(NFRDA, 1986). In Table 1, H_1 is the thickness of the upper layer in the East Sea, which represents the thermocline depth. H_2 is representative of the depth range of the strongest subsurface currents. T_o is also set

Table 1. Parameters for all the ocean models used in this study

H_1	initial upper-layer thickness	60 m
H_2	initial lower-layer thickness	240 m
H_e	starting depth of entrainment	60 m
T_0	initial temperature of upper layer	12°C
T_d	temperature of deep layer,1½-layer model	4°C
T_2	temperature of the second layer, 2½-layer model	4°C
T_3	temperature of deep layer, 2½-layer model	1°C
ε	coefficient of thermal expansion	3×10^{-4} °C^{-1}
t_e	thermodynamic time constant	1/8 day
t_h	heating time constant	50 days
ν_h	horizontal mixing coefficient	2×10^6 cm^{2}s^{-1}
k_h	horizontal diffusion of heat	2×10^7 cm^{2}s^{-1}
g	gravity acceleration	980 cm^{2}s^{-1}
$\triangle x$	grid space (= $\triangle y$)	10 km
$\triangle t$	time interval	20 min

as a realistic value in the East Sea and 12℃ is the typical value in the vicinity of 38°N for the East Sea in the winter season, and T_2 is a typical temperature of the deep ocean. The coriolis parameter (f) was calculated for each grid box. While the wind forcing strengthened, the vertical and horizontal mixings became active. Vertical mixing was also necessary in order to include wind stress effects. In general, the horizontal eddy viscosity ν_h and horizontal diffusion of heat k_h were taken to be constant with values of $2 \times 10^6 \sim 2 \times 10^7$cm^{2}s^{-1}. The values of ε, t_e and t_h can affected the numerical solutions, however, in the present study the numerical solutions were not sensitive to these values according to various additional preliminary experiments.

The model ocean was forced by wind fields similar in strength and structure to the wind over the East Sea during the winter season, as in Kim et al. (1998). The wind fields had separable forms as follows:

$$\tau^x = \tau_0 X(x) Y(y) T(t)$$
$$\tau^y = -\tau_0 X(x) Y(y) T(t),$$

where τ^x and τ^y are the offshore and alongshore components, respectively. The negative sign (-) means the northerly wind and X, Y and T are the offshore, alongshore, and temporal structures of wind fields, respectively. For determining the

spatial-temporal structure of the wind fields used in this model, the distribution pattern of the winds on the East Sea in the analysis by Kim et al. (1998) was refferred.

Fig. 3 illustrates the wind fields that forced the model ocean in this study. It shows the locations of the wind fields as well as their spatial and temporal structures, $X(x)$, $Y(y)$, and $T(t)$. The wind fields included three components; a background wind field τ^x_B in the offshore direction, an along-shore wind τ^y hat represented the moderate northerly and northwesterly wind in the winter season, and an offshore wind patch τ^x_J. Fig. 3a shows the spatial structure. The maximum value of the wind stress in the background wind field τ^x_B was 1 dyne/cm^2 at 39°N, which decreased smoothly in both southward and northward directions relative to 39°N, and finally became zero at the northern and southern boundaries. The background wind was cut off offshore near the eastern boundary. The northerly wind stress had an initial magnitude of 1 dyne/cm^2 between 42°N and 39.6°N, then decreased gradually in a southward direction, and finally became zero at 38.4°N. Furthermore, its magnitude was essentially uniform relative to the offshore distance. The wind patch τ^x_J was 1.2° wide and 200 km offshore. It was centered at 39°N with a maximum value of 4 dyne/cm^2. As a result, the total wind stress field (τ^x_B + τ^y + τ^x_J) repre-

senting the wind behavior during the peak phase of the northwest monsoon, can be shown in Fig. 3b. Fig. 3c shows the temporal structure $T(t)$ of the maximum strength variation of τ^x_B, τ^y, and τ^x_J, with $t=0$ corresponding to December 1. The temporal structure $T(t)$ of τ^y and background wind fields τ^x_B increased smoothly for the first 15 days, and then remained constant from day 15 until day 75, after which point they gradually relaxed to zero
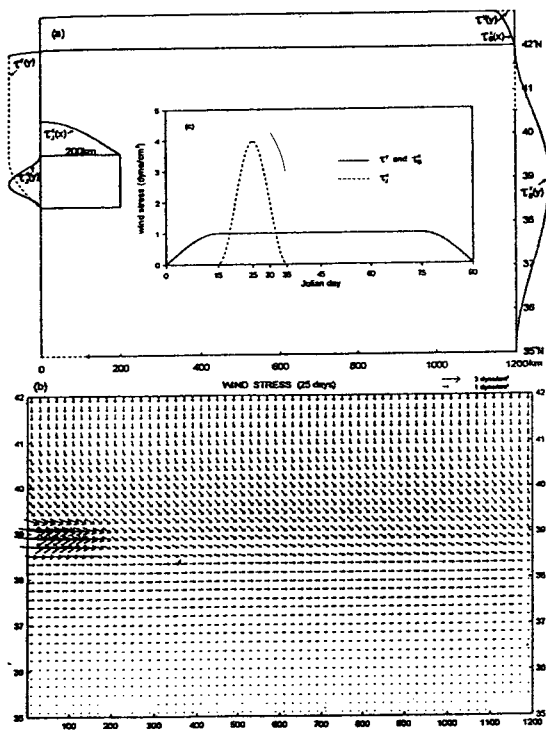

Fig. 3. A schematic diagram illustrating the spatial (a and b) and temporal (c) structure of the wind field.

until day 90. The $T(t)$ of wind patch τ^x_J increased and decreased with the cosine function from day 15 to day 35. The maximum value of the wind stress was, therefore, about 5 dyne/cm^2 at 39°N on day 25.

3. Results and Discussion

This study investigated the evolution processes of the Sokcho and Ulleung Eddies, their interaction, and the Eddy-Tsushima Current interaction using a nonlinear 2½-layer numerical model

though realistic observations about the mesoscale phenomena in the East Sea are not clear. The 2½-layer model solutions were then compared with the solutions from a nonlinear 1½-layer model. The model ocean for both cases was initially motionless, then simultaneously forced by strong offshore winds for 20 days and alongshore winds for 90 days, and also allowed the inflow of the Tsushima Current for 360 days.

After 30 days (Fig. 4), anticyclonic and cyclonic gyres were developed due to the strong wind stress curl on both sides of the offshore wind axis between 38.4°N and 39.6°N, as in Kim et al. (1998). A southward coastal current with a speed of about 15 cms^{-1} was transiently developed along the northern and western boundaries due to the northerly wind. The inflow was deflected eastward right after entering the basin due to the coriolis force and nonlinear self advection, and then continued flowing to the east along the southern boundary as a coastal current. The velocity fields in the 1½-layer model (Fig. 4a) were similar to those in the 2½-layer model. However, the southward coastal current along the western boundary in the upper layer of the 2½-layer model (Fig. 4b), was considerably weakened due to the northward coastal current of the lower layer. The velocity field in the lower layer (Fig. 4c) was very similar to that in the upper layer except that a northward coastal current with a speed of 10 cms^{-1} was induced due to the geostrophic balance. A symmetrical counter-rotating circulation appeared at the peak of the local winds.

After 60 days (Fig. 5), the anticyclonic eddy with a horizontal dimension of about 150 km developed due to the nonlinear advection term. In this study, this anticyclonic eddy is named the Sokcho Eddy. All the regions where h was less than H vanished because of entrainment, so that the cyclonic eddy almost disappeared. The inflow penetrated somewhat further to the north compared to day 30 and then deflected eastward. In the 1½-layer model (Fig. 5a), the Sokcho Eddy was almost circular in shape and its center (X_m, Y_m) was located at $X_m = 70$ km and $Y_m = 38.3$°N. The southward coastal current nearly disappeared on the southern part of the anticyclonic eddy and a northward coastal current along the western boundary was
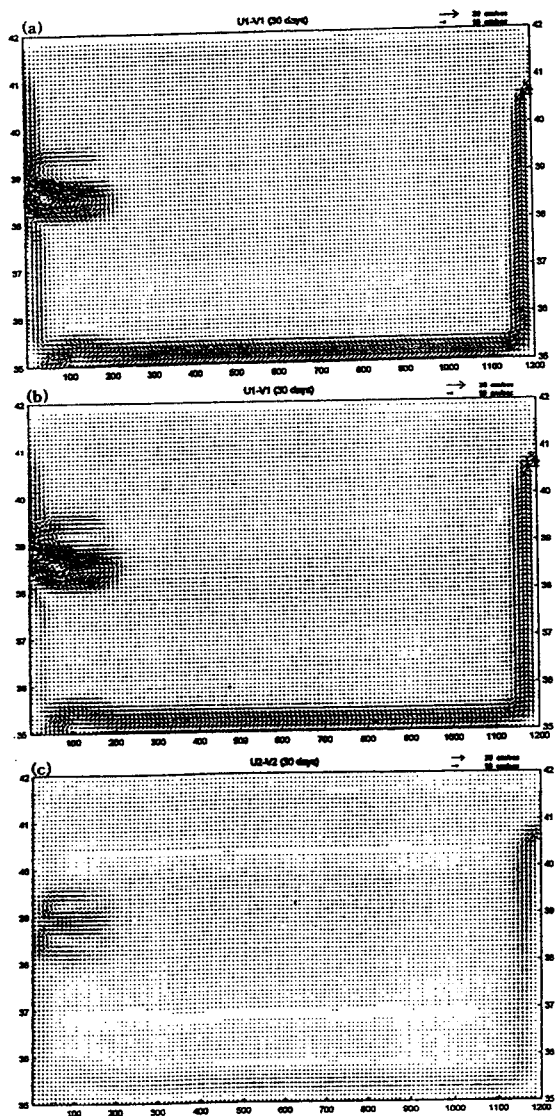
Fig. 4. Current field of the upper layer (a) by 1½-layer (b) and lower layer (c) by 2½-layer model at day 30.

Fig. 5. As in Fig. 4 except at day 60.

generated by the inflow of the Tsushima Current. In the 2½-layer model (Fig. 5b), the Sokcho Eddy was completely circular in shape and its center was located at X_m = 130 km and Y_m = 38.2°N. In the ower layer (Fig. 5c), very weak return coastal currents developed along the eastern and southern boundaries, accordingly, the northern boundary current along the eastern boundary was weakened. When comparing the two cases, the Sokcho Eddy was located at the western boundary in the 1½

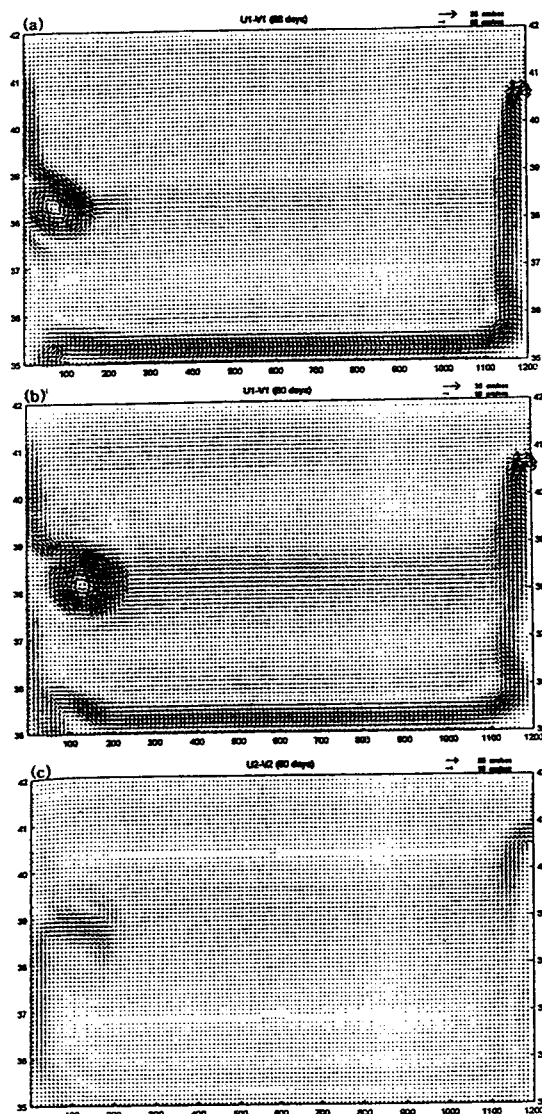-layer model, whereas, in the 2½-layer model it was somewhat offshore due to an eastward subsurface current. Unlike the 1½-layer model, a northward coastal current developed along the western boundary in the 2½-layer model due to a subsurface northward coastal current. In addition, the generating location of the Sokcho Eddy was close to the results of other real observation studies (Min et al., 1995; Lee et al., 1995; Kim, 1995).

After 90 days (Fig. 6), when the background winds stopped, the northward coastal current along the western boundary became stronger due to the

disappearance of the wind patch. It overshot near 39.3°N, deflected to the east due to the wind stress curl, and then flowed eastward out through the eastern exit with a meandering motion. As a result, a polar front was formed between 38°N and 39°N. In the $1\frac{1}{2}$-layer model (Fig. 6a), the center of the Sokcho Eddy was located at X_m = 90 km and Y_m = 38.2°N and its horizontal size was about 160 km. In the upper layer (Fig. 6b) of the $2\frac{1}{2}$-layer model, the center of the Sokcho Eddy was located mear X_m = 150 km and Y_m = 37.9°N and its horizontal size was about 150 km. The overall features in the lower layer (Fig. 6c) were very similar to those in the upper layer except for a strong return current along the eastern and southern boundaries. In the $2\frac{1}{2}$-layer model (Fig. 6b), there was an additional weak cyclonic circulation in the northern part of the polar front because the eastward current was much stronger than that in the $1\frac{1}{2}$-layer model and the southern boundary current became weak as a result of the return currents in the lower layer. Furthermore, the northward flow along the western boundary in the $2\frac{1}{2}$-layer model wrapped and strengthened the Sokcho Eddy more than in the $1\frac{1}{2}$-layer model due to a subsurface current, as a result the eddy in the $2\frac{1}{2}$-layer model was stronger and bigger. According to Lee *et al.* (1995), the strong northward EKWC, called a warm streamer, enhances and wraps the circular Sokcho Eddy. Accordingly, the result of the $2\frac{1}{2}$-layer model is closer to real observation results.

After 120 days (Fig. 7), as the maximum speed of the inflow through entrance increased, the northward flow of the Tsushima Current increased significantly. This flow became the EKWC and strengthened the Sokcho Eddy. In the $1\frac{1}{2}$-layer model (Fig. 7a), the eastward current along the southern boundary became considerably stronger. The maximum speed was 46 cms^{-1} at the entrance. In the $2\frac{1}{2}$-layer model (Fig. 7b), the eastward coastal current along the southern boundary became weaker than that in the $1\frac{1}{2}$-layer model because most of the EKWC flowed northward due to a strong subsurface current thereby enhancing the Sokcho Eddy.

After 180 days (Fig. 8), the inflow penetrated further to the north and the clockwise deflection of the inflow increased. In the $1\frac{1}{2}$-layer model
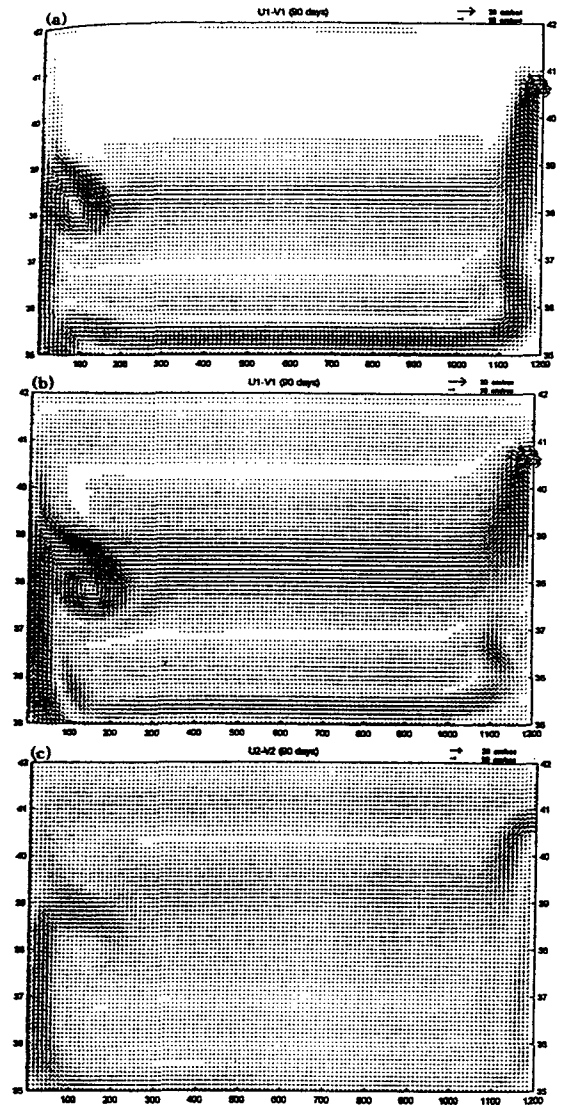

Fig. 6. As in Fig. 4 except at day 90.

(Fig. 8a), the EKWC made the Sokcho Eddy more elliptical in shape. The center of the Sokcho Eddy was located at X_m = 90 km and Y_m = 38.1°N. In the $2\frac{1}{2}$-layer model (Fig. 8b), the northward coastal current became stronger and made the Sokcho Eddy more circular in shape. A weak eastward meandering current on the eastern side of the Sokcho Eddy was also evident. After 240 days (Fig. 9), the anticyclonic eddy near the Korea strait, changed to become an enclosed eddy, as in Kim *et al.* (1997a). In this study, this anticyclonic
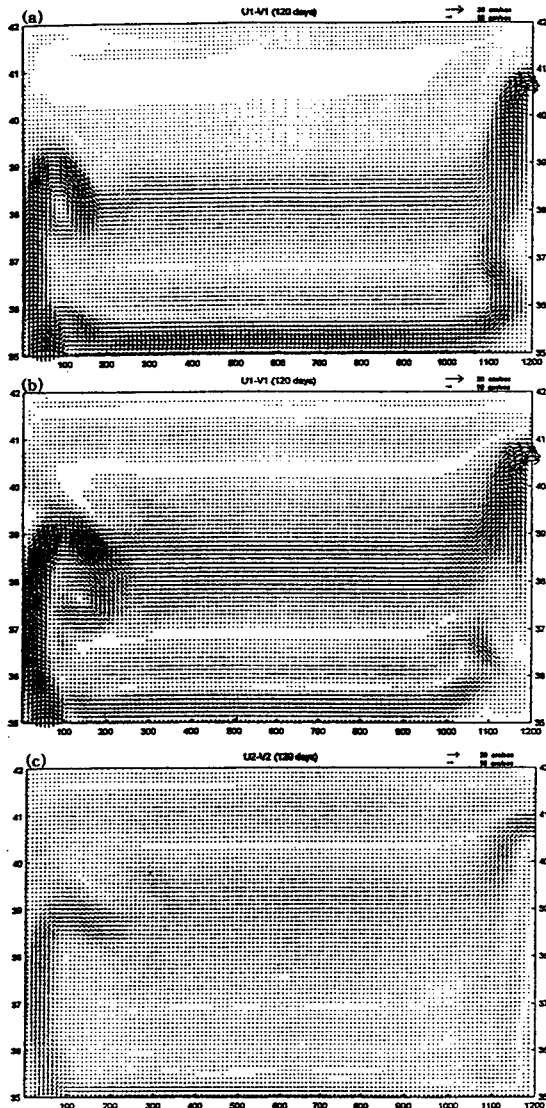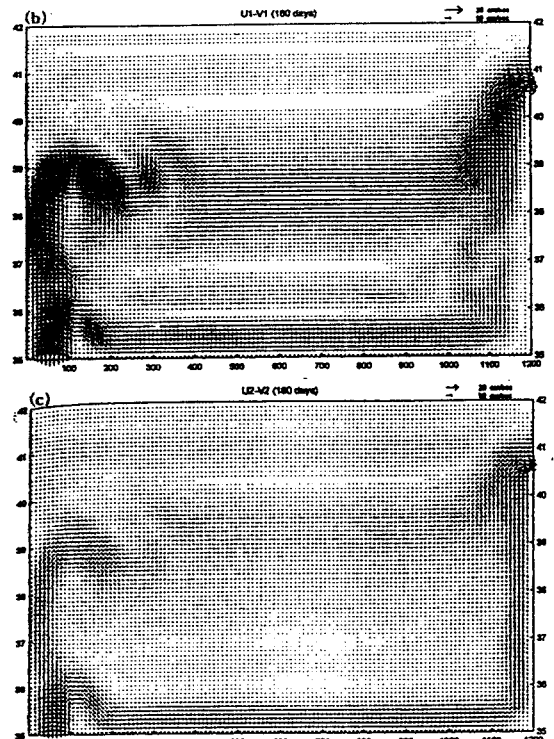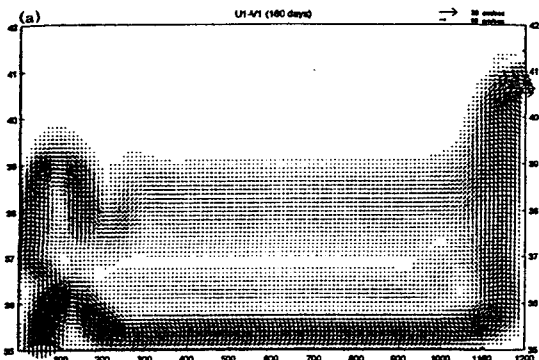
Fig. 7. As in Fig. 4 except at day 120.

Fig. 8. As in Fig. 4 except at day 180.

eddy is called the Ulleung Eddy and its generating location was found to be similar to that of other real observations, as with the Sokcho Eddy. Therefore, the Sokcho and Ulleung eddies clearly exist along the western boundary. With time, the Ulleung Eddy moved slowly to the north. In contrast, the Sokcho Eddy neither moved nor changed its size in spite of variations in the inflow. In the 1½-layer model (Fig. 9a), the Ulleung Eddy changed its circular shape to 200 km in a zonal direction. The center of the Ulleung Eddy was located at $X_m = 140$ km and $Y_m = 35.6°N$. Whereas, in the 2½-layer model (Fig. 9b), the 150 km diameter Ulleung Eddy changed to an elliptical shape in a meridional direction due to the strong EKWC. The centers of the Sokcho and Ulleung eddies were about $X_m = 120$ km and $Y_m = 38.3°N$, and $X_m = 110$ km and $Y_m = 35.7°N$, respectively. The eastward meandering current became stronger and more evident, and by day 240 its wavelength increased to about 160 km.

After day 300 (Fig. 10), the Ulleung Eddy gradually moved to the north. In the 1½-layer model (Fig. 10a), the center of the Ulleung Eddy was
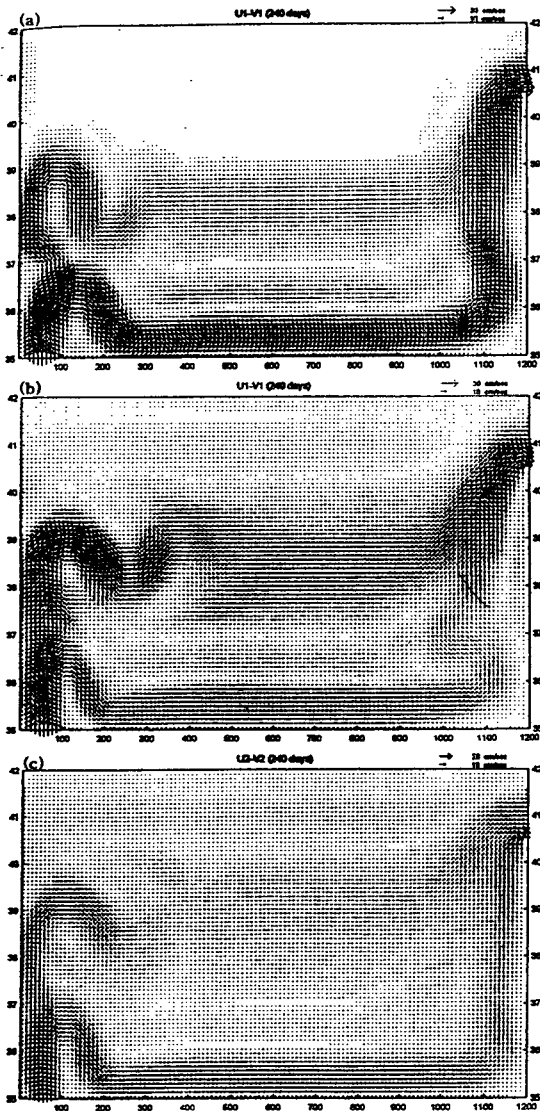
Fig. 9. As in Fig. 4 except at day 240.

located at X_m = 140 km and Y_m = 35.9° N and its horizontal size was about 210 km. In the 2½ -layer model (Fig. 10b), the Ulleung Eddy gradually changed to a more elliptical shape due to the EKWC. The centers of the Sokcho and Ulleung eddies were at X_m = 130 km and Y_m = 38.2° N, and X_m = 105 km and Y_m = 36.2° N, respectively. The diameters of the Sokcho and Ulleung eddies were about 160 and 150 km, respectively. The 1½-layer model showed most of the EKWC forming the Ulleung Eddy, accordingly, its scale and strength

were larger than the Sokcho Eddy, plus the eastward coastal current was very strong due to a channelling effect, as illustrated by Wang(1987). While in the 2½-layer model, most of the EKWC went further north due to a strong northward coastal current in the lower layer. As a result, the scale and strength of the Sokcho Eddy were larger than the Ulleung Eddy in the 2½-layer model, plus the eastward meandering current was also clearer than in the 1½-layer model. Therefore, the characerics of the two eddies in the 2½-layer model were different to those in the 1½-layer model due to the existence of a strong subsurface current. In addition, after 300 days, as the velocity of the inflow decreased, the Ulleung Eddy in the 2½-layer model became weaker and changed into an elliptical shape in a meridional direction due to the strong EKWC. Whereas, in the 1½-layer model, the Ulleung Eddy increased in size and gradually changed into a circular shape.

In the 1½-layer model (Fig. 11a), after day 360, most of the EKWC wrapped the Ulleung Eddy. As a result, the Ulleung Eddy was considerably stronger and its size was about 230 km. The center of the Ulleung Eddy was located at X_m = 130 km and Y_m = 36.1° N. Whereas the Sokcho Eddy and the meandering were relatively weak after day 330 because of a weakened EKWC. Accordingly, this model successfully revealed the Sokcho and Ulleung eddies. However, the two eddies had no interaction with each other. In contrast, in the 2½ -layer model (Fig. 11b), the EKWC was still strong due to a subsurface current. The Ulleung and Sokcho eddies did interact with each other and the Ulleung Eddy was seemingly absorbed by the Sokcho Eddy when the EKWC was relatively strong. Kundu (1990) suggested the superposi- tioning of the two neighboring vorticities rotating in the same direction. As per Kundu's illustration, the Sokcho and Ulleung Eddy are superpositioned in Fig. 11b. In addition, Lee and McCreary (1996, not published) cleary represented in a numerical experiment that two westward moving anticyclonic eddies, generated due to strong offshore winds in the Gulfs of Tehuantepec and Papagayo, finally

became one eddy due to the superpositioning of the two eddies.

Fig. 12 shows the horizontal temperature distribution at a depth of 200 m off the east coast of Korea in April and June 1997. In April (Fig. 12a), the Sokcho and Ulleung eddies exhibited a fully developed circular shape, although the generating locations of the two eddies were somewhat south compared to the results of other studies (Kim, 1993; Lee *et al.*, 1995; Lie *et al*, 1995). While, in
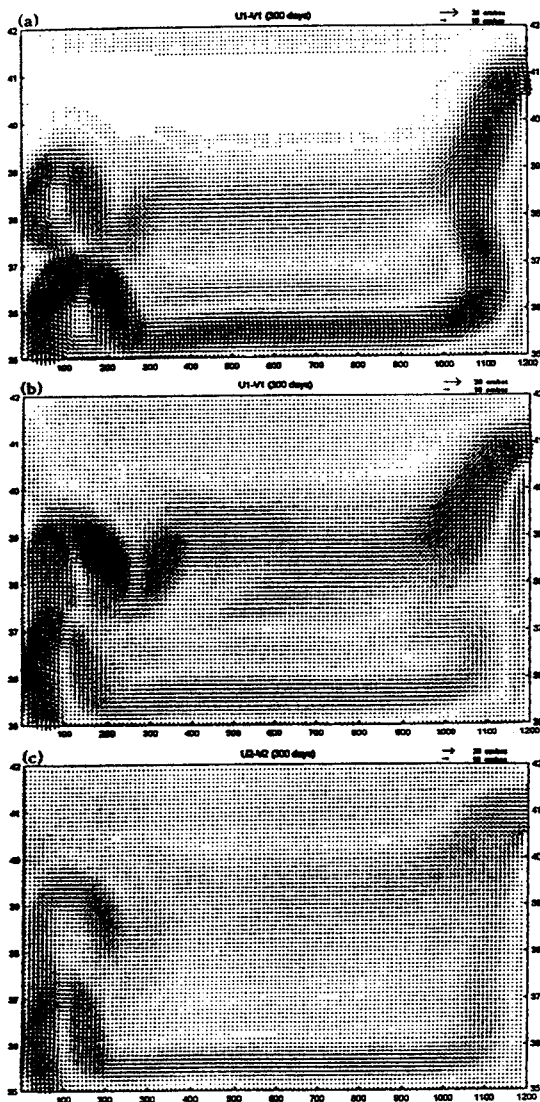

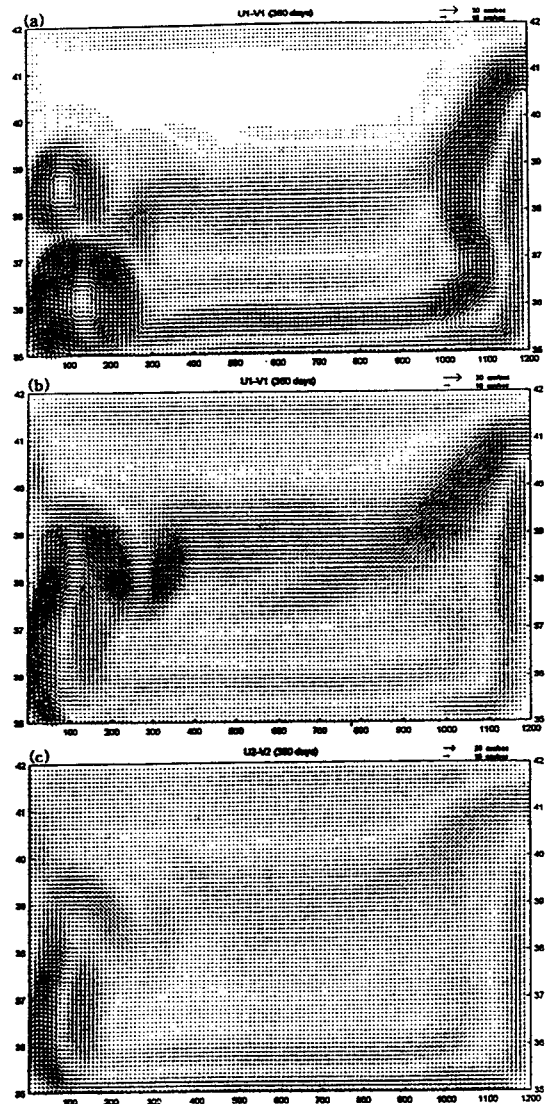Fig. 10. As in Fig. 4 except at day 240.

Fig. 11. As in Fig. 4 except at day 360.

June (Fig. 12b) the two eddies moved north and closer to each other, which seems to be the first step towards their mutual interaction.

4. Summary

Nonlinear 1½-layer and 2½-layer models were used to investigate the evolution processes of mesoscale Sokcho and Ulleung eddies, the interaction between the two eddies, and the Eddy-Tsushima Current interaction in the East Sea. The model ocean allowed for strong local offshore winds
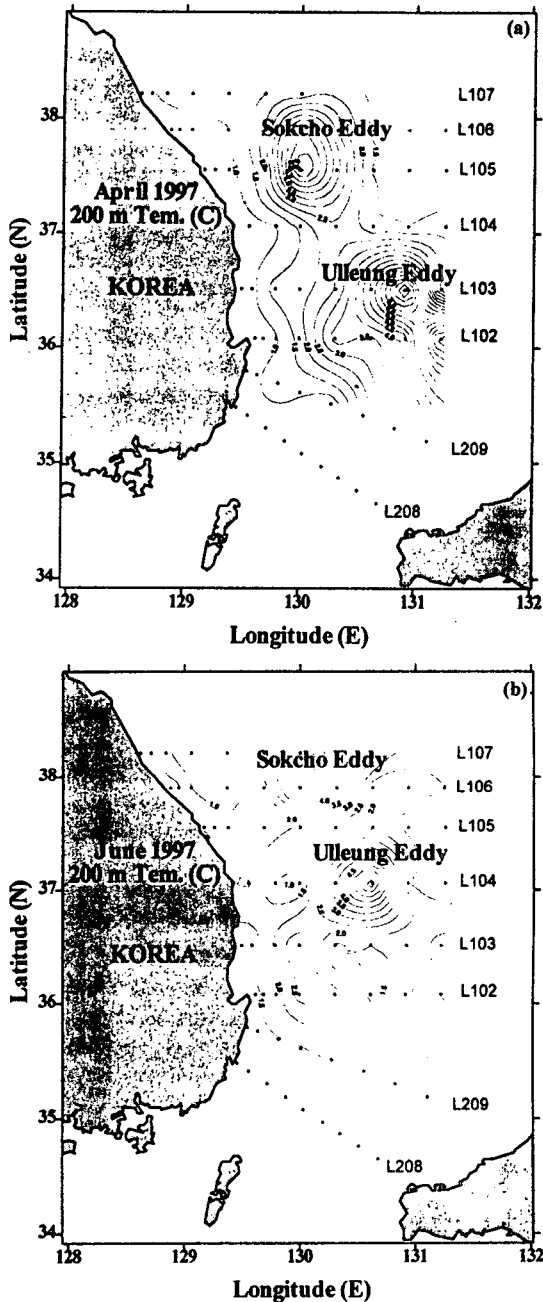
Fig. 12. Horizontal distributions of temperature at 200 m depth off the east coast of Korea on April (a) and June (b), 1997.

and a seasonal inflow variation of the Tsushima Current through the Korea Strait.

According to this numerical study, an anticyclonic eddy of about 150 km in diameter was pro-

duced by strong local offshore winds near the western boundary in the East Sea, as in Kim et al. (1998). A meandering to the east developed on the eastern side of the strong anticyclonic eddy (the Sokcho Eddy). The Sokcho Eddy was almost stationary at latitude between 37.5～39.0°N. In the $1\frac{1}{2}$-layer model, the Sokcho Eddy was located near the western boundary, whereas in the $2\frac{1}{2}$-layer model, it was somewhat offshore due to eastward subsurface currents, which is closer to real observations. The Ulleung Eddy was also produced between 35.0～37.0°N by the seasonal variation of the Tsushima Current and its nonlinear self-advection, as in Kim et al. (1997a). In the summer season, the mass transport of the inflow increased and the Tsushima Current went northward as a EKWC. When the background winds stopped, this northward coastal current (EKWC) then wrapped and strenghened the Sokcho Eddy generated by local offshore winds.

In the $2\frac{1}{2}$-layer model, the EKWC went further northward due to a strong subsurface currrent, thereby wrapping and strengthening the Sokcho Eddy, accordingly, it made the Sokcho Eddy more circular in shape, its scale and strength were larger that the Ulleung Eddy and a meandering was clearly developed. Whereas, in the $1\frac{1}{2}$-layer model, most of the EKWC wrapped and strengthened only the Ulleung Eddy. Therefore, the Sokcho Eddy and its meandering were considerably weaker, plus the scale and strength of the Ulleung Eddy were larger than the Sokcho Eddy.

The Sokcho and Ulleung Eddies were successfully produced by the nonlinear $1\frac{1}{2}$ and $2\frac{1}{2}$-layer numerical models. In the $2\frac{1}{2}$-layer model especially, a weak cyclonic circulation appeared in the northern part of the polar front because some of the eastward current did not flow out through the exit. Over time the Sokcho and Ulleung Eddies became weak and began interacting with each other after 360 days, finally the Ulleung Eddy disappeared and absorbed by the relatively strong Sokcho Eddy. In contrast, in the $1\frac{1}{2}$-layer model, the two eddies did not interact and no weak cyclonic circulation appeared in the northern part of the polar front. These layer models did not show a realistic temperature profile, because the temperature of the Tsushima Current was not the focus of the model ocean.

5. References

[1] Kim, C. Ed., 1993, *A Study on the mesoscale warm eddy in the southwestern part of the East Sea*. Ministry of Science and Technology, Seoul, BSPN 00187-611-1, 84pp (in Korean).

[2] Kim, S. Y., 1995, *Numerical experiments on the generation of the mesoscale eddies off the east coast of Korea*. Thesis of Ph.D., Nat. Fish. Univ., Pusan, 128 pp.

[3] Kim, S. Y., J. C. Lee, H. S. Lee and T. B. Shim, 1997a, Numerical Experiment on the Ulleung Eddy due to the variation of the Tsushima Current in the East Sea. *J. Kor. Fish. Soc.* 30, 1033-1043.

[4] Kim, S. Y., J. C. Lee, H. S. Lee and T. B. Shim, 1997b, Triggering effect of the polar front on the eddies in the East Sea. *J. Kor. Fish. Soc.* 30, 1044-1045.

[5] Kim, S. Y., H. S. Lee and J. C. Lee, 1998, Numerical experiment on the Sogcho Eddy due to the strong offshore winds in the East Sea. *J. Fish. Sci. Tech.* 1, 7-18.

[6] Lee, J. C., D. H. Min, T. B. Shim, H. S. Lee and H. S. Yang, 1995, The Sogcho Eddy, I: Observation on May 1992. *J. Kor. Fish. Soc.* 28, 354-364.

[7] Lie, H. J., S. K. Byun, I. K. Bang and C. H. Cho, 1995, Physical structure of eddies in the Southwestern East Sea. *J. Oceanogr.*, 30, 170-183.

[8] Lim, K. S. and K. Kim, 1995. A numerical study on the interaction of Ulleung Warm Eddy with topography and lateral boundary. *J. Oceanogr. of Korean*, 30, 565-583.

[9] McCreary, J. P., H. S. Lee and D. B. Emnfield, 1989, The response of the coastal ocean to strong offshore winds: with application to circulation in the Gulfs of Tehuantepec and Papagayo. *J. Mar. Res.*, 47, 81-109.

[10] McCreary, J. P., and P. K. Kundu, 1998, A numerical investigation of the Somali Current during the south west monsoon. *J. Mar. Res.*, 46, 25-58.

[11] Min, D. H., J. C. Lee, T. B. Shim, and H. S. Lee, 1995, Eddy distribution off the East Coast of Korea derived from satellite infrared imagery. *J. Kor. Fish. Soc.* 28, 354-364.

[12] National Fisheries Research and Development Agency of Korea, 1986, *Mean oceanographic charts of the adjacent seas of Korea*. NFRDA, Korea, 186 pp (in Korean).

[13] Kundu, P. K., 1990. *Fluid Mechanics*. Academic Press Inc., SanDiego, 638pp.

[14] Shin, H. R., S. K. Byun, C. Kim, S. Hwang, and C. W. Shin, 1995, The characteristic of structure of warm eddy observed to the northwest of Ulleung do in 1992. *J. Oceanogr. Soc. Korea*, 30, 39-56.

[15] Wang, D. P., 1987, The strait surface outflow. *J. Geo. Res.*, 92, 10,807-10,825.